J Nanopart Res (2019) 21:184
https://doi.org/10.1007/s11051-019-4628-9

RESEARCH PAPER

Cellular uptake and cytotoxicity of unmodified Pr^{3+}:LaF_3 nanoparticles

Maksim S. Pudovkin · Pavel V. Zelenikhin · Victoria V. Shtyreva · Vladimir G. Evtugyn · Vadim V. Salnikov · Alexey S. Nizamutdinov · Vadim V. Semashko

Received: 23 April 2019 / Accepted: 5 August 2019

Abstract Pr^{3+}:LaF_3 ($C_{Pr} = 1\%$) nanoparticles were characterized by means of transmission electron microscopy (TEM), X-ray diffraction, energy-dispersive spectroscopy, and optical spectroscopy. The obtained 14 nm Pr^{3+}:LaF_3 ($C_{Pr} = 1\%$) crystalline hexagonal-structured nanoparticles contain Pr, La, and F only. The luminescent spectra emission bands corresponded to the emission bands of Pr^{3+}ions. The Pr^{3+}:LaF_3 ($C_{Pr} = 1\%$) nanoparticles effectively interact with A 549, LEC, and MDCK cells. By means of TEM, it was revealed that after 2 h of the nanoparticle exposure, A 549, MDCK, and LEC cells internalized the nanoparticles and 20–300 nm agglomerates of the nanoparticles packed into 200–500 nm vesicles were found into the cytoplasm. It seems that the internalization occurs via macropinocytosis. In A 549 cells, some vesicles were disrupted and the nanoparticles escaped the vesicles floating freely in the cytoplasm. Flow cytometry showed that all the cells effectively interact with nanoparticles. This interaction leads to cell granularity change. Specifically, A 549, MDCK, and LEC, and cells treated by nanoparticles have the values of size scattered signal 16 ± 2, 20 ± 3, and $39 \pm 3\%$, respectively, comparing with the untreated cells. The Pr^{3+}:LaF_3 ($C_{Pr} = 1\%$) nanoparticles were not found into the cellular organelles. The cytotoxicity of the Pr^{3+}:LaF_3 ($C_{Pr} = 1\%$) nanoparticles is not significant at concentrations of 0.05, 0.1, 0.25, and 0.5 g/L.

Keywords Pr^{3+}:LaF_3 nanoparticles · Fluoride nanoparticles · Cytotoxicity · Cellular uptake · Flow cytometry · Macropinocytosis · Nanobiomedicine

Introduction

In modern life, luminescent nanomaterials are widely used in different branches of science and industry (Gnach et al. 2015; Nel et al. 2009; Lellouche et al. 2012). Among the huge variety of luminescent nanomaterials, rare earth (RE)-doped fluoride nanoparticles hold a special place mainly because of their excellent photostability, long luminescent lifetimes (micro- to milliseconds), sharp emission bands, high chemical stability, and lack of photobleaching (Dong et al. 2015; Jalil and Zhang 2008; Ximendes et al. 2016; Bekah et al. 2016). Indeed, the RE doper fluoride nanoparticles demonstrate their applicability in bioimaging (Dong et al. 2015), hyperthermia with subcutaneous

Electronic supplementary material The online version of this article (https://doi.org/10.1007/s11051-019-4628-9) contains supplementary material, which is available to authorized users.

M. S. Pudovkin (✉) · A. S. Nizamutdinov · V. V. Semashko
Institute of Physics, Kazan Federal University, Kremlevskaya 18, Kazan, Russian Federation 420008
e-mail: jaz7778@list.ru

P. V. Zelenikhin · V. V. Shtyreva
Institute of Fundamental Medicine and Biology, Kazan Federal University, Kremlevskaya 18, Kazan, Russian Federation 420008

V. G. Evtugyn · V. V. Salnikov
Interdisciplinary Center for Analytical Microscopy, Kazan Federal University, Parizhskoy Communi 9, Kazan, Russian Federation 420008

Published online: 17 August 2019

thermal sensing (Ximendes et al. 2016), "hybrid" radiotherapy–photodynamic therapy (Bekah et al. 2016), protection of cells against oxidative stress (Shcherbakov et al. 2015), temperature sensing of a single cell (Jaque and Vetrone 2012), etc. For all these biomedical applications, the toxicology concerns and features of interaction between nanoparticles and living cells should be studied as thoroughly as possible. It is noteworthy that in biomedical applications the nanoparticles are usually coated by biocompatible polymers. However, the efficiency of coating procedure is still a matter of concern and some nanoparticles may remain uncoated. More importantly, the lifetime of such coating into harsh physiological conditions is not predicted and depends on many factors. Hence, the studying of toxicity and cellular uptake of bare unmodified nanoparticles is fundamental and prior tack before taking into consideration the coating.

Unlike relatively well-studied toxicity of Au, Ag, SiO, TiO_2, ZnO, and CdSe nanomaterials, the toxicity of RE-doped nanoparticles, including fluoride ones, is not well studied yet (Nel et al. 2009). Although the previous study revealed low toxicity of some fluoride nanoparticles (Xing et al. 2012; Wang et al. 2013; Shcherbakov et al. 2015; Gnach et al. 2015; Wysokińska et al. 2016), additional study is still required. In particular, in Xing et al. (2012), it is shown that Tm^{3+}:$NaYbF_4$ nanoparticles demonstrate very low toxicity toward human liver cells (HL 7702) and murine macrophage cells (RAW264.7). It is shown in Jalil and Zhang (2008) that silica-coated Yb^{3+}/Er^{3+}:$NaYF_4$ nanoparticles demonstrate negligible toxicity toward bone marrow-derived mesenchymal stem cells, and it is proved that these nanoparticles do not cause membrane damage. A work (Zhou et al. 2011) also confirms low toxicity of citrate-capped $Gd^{3+}/Yb^{3+}/Er^{3+}$:$NaYF_4$ nanoparticles toward the human nasopharyngeal epidermal carcinoma cell line KB cells. It was proven that these nanoparticles penetrate the cell membrane of living KB cells. On the other hand, PIE-coated Yb^{3+}/Er^{3+}:$NaYF_4$ nanoparticles cause cell membrane disruption because of the positively charged PIE coat. It should be mentioned that in all these cases, in vitro toxicity is estimated via calorimetric MTT assay. In addition to the nanoparticle toxicity, type of cell exposed to the nanoparticles also plays an important role in toxicity. This is due to the variation in cell physiology (epithelial or lymphoid), proliferation state (tumoral or resting cells), membrane characteristics, and phagocyte characteristics among different cell types. According to the literature data, unmodified RE-doped fluoride nanoparticles are easily internalized by living cells. For example, in Shcherbakov et al. (2015), it was proved that unmodified Tb^{3+}:CeF_3 nanoparticles are internalized by HeLa cervical cancer cells even after 5 min of nanoparticle exposure. Nanoparticles are internalized by different types of endocytosis that differ by mechanism, size, and type of cargo to mention a few. The four major types of endocytosis recognized are phagocytosis, pinocytosis, clathrin-mediated endocytosis, and caveolae-mediated endocytosis (Oh and Park 2014; Ribeiro et al. 2016). Furthermore, the definition of a type of endocytosis and its efficiency remain a very important task.

Although, the RE-doped $NaLnF_4$ (Ln = Y, Gd) nanoparticles are considered very efficient nanomaterials, the RE-doped trifluoride (LnF_3 (Ln = Ce, La)) are no less effective for a broad list of applications.

It seems that toxicity of RE-doped $NaLnF_4$ (Ln = Y, Gd) is relatively well-studied. Also, there have been the reports on the low toxicity of trifluoride CeF_3 nanoparticles (Shcherbakov et al. 2015). However, toxicology studies of LaF_3, as well as other trifluorides, are rather rare (Wang et al. 2013). In turn, the discussed RE-doped $NaLnF_4$ (Ln = Y, Gd) nanoparticles can significantly differ from trifluoride (LnF_3 (Ln = Ce, La)) ones by surface charge density. Indeed, the surface charge density of nanoparticles plays an important role in the interaction of nanoparticles with living cells (Nel et al. 2009). It was reported in Ladol et al. (2016) that the charge density of the surface of the $NaLaF_4$ highly depends on the ionic radius of the doping ions which replace the La^{3+} in $NaLaF_4$. Moreover, the ionic radii of Na^+ (0.227 nm), Y^{3+} (0.101 nm), and Gd^{3+} (0.105 nm) are significantly less than ionic radii of Ce^{3+} (0.248 nm) and La^{3+} (0.250 nm). The surface charge density of trifluoride (LnF_3 (Ln = Ce, La)) and $NaLnF_4$ (Ln = Y, Gd) nanoparticles is different. According to these conclusions, it is believed that the features of interaction of trifluoride (LnF_3 (Ln = Ce, La)) with living cells differ from these features for $NaLnF_4$ (Ln = Y, Gd) nanoparticles. Hence, the safe industrial and scientific operation standards or recommendations for $NaLnF_4$ (Ln = Y, Gd) nanoparticles cannot be extrapolated to the working with trifluoride (LnF_3 (Ln = Ce, La)) nanoparticles. The additional studies of trifluoride (LnF_3 (Ln = Ce, La)) are highly demanded.

In this work, we focus on studying of toxicity and cellular uptake of Pr^{3+}:LaF_3 nanoparticles toward lung

carcinoma (A 549), Madin–Darby canine kidney (MDCK), and lung epithelial of a cow (LEC).

Pr^{3+}:LaF_3 nanomaterials are considered very promising in a broad list of biomedical applications (Pudovkin et al. 2016). It has been reported in Rai et al. (2006), Kamma et al. (2009), Kaczkan et al. (2013), Pudovkin et al. (2017), Pudovkin et al. (2019), and Rakhmatullin et al. (2019) that because of thermally coupled $^3P_1$ to $^3P_0$ electronic states of Pr^{3+} ions Pr^{3+}-doped nanomaterials can be used as nanothermometers operating into broad temperature range including physiological one. These facts pave the way toward thermal sensing of a single cell in vitro (Yang et al. 2011; Pudovkin et al. 2018) toward some other biomedical and industrial applications. The emission spectrum of Pr^{3+} in lanthanum fluoride host matrix overlaps with photosensitizers, such as acridine ($C_{13}H_9N$) and cyanine, which are highly relevant in "hybrid" radiotherapy–photodynamic therapy (PDT) mentioned previously.

The main goal of this work is to provide additional information concerning the cytotoxicity of Pr^{3+}:LaF_3 nanoparticles and features of their interaction with eukaryotic cells (Semashko et al. 2018).

Materials and methods

Synthesis and characterization of Pr^{3+}:LaF_3 (C_{Pr} = 1%) nanoparticles

The Pr^{3+}:LaF_3 (C_{Pr} = 1%) nanoparticles were synthesized via the co-precipitation method (Pudovkin et al. 2018 Alakshin et al. 2014, 2016). In order to synthesize Pr^{3+}:LaF_3 (C_{Pr} = 1%) nanoparticles, 0.04 g of Pr_2O_3 and 4.00 g and La_2O_3 were added to 85 mL of 10% nitric acid in a glass beaker. Both mixtures were heated to 50 °C and stirred for 45 min until a transparent solution appeared. Then, the mixtures were filtered, poured in polypropylene glasses, and put on magnetic mixers (400 rpm). The solutions of NaF were prepared by adding 3.8 g of NaF into 500 mL of distilled water. The NaF solution was swiftly poured. Then, the pH was adjusted to 4 by adding a 25% solution of ammonium hydrate. Then, the mixture was stirred for 30 min (400 rpm) and washed by centrifugation (Janetski K24; 12,000 RPM) using deionized water for several times. Then, the 10.0 g/l colloidal solution of the nanoparticles was obtained. The hydrodynamic radii were measured via DLS. In order to obtain a colloidal solution of the nanoparticles into the Eagle's (MEM) biological medium, the nanoparticle suspension in distilled water was added to the cultural medium in a ratio of 1/10 (*v*/*v*), and, then, the size distribution was measured via DLS.

The phase composition of the material was characterized by an X-ray diffraction method with Shimadzu XRD-7000S X-ray diffractometer.

In order to measure nanoparticle sizes and the rate of nanoparticle agglomeration in different mediums, the size distributions and average hydrodynamic radii in water and minimum essential medium Eagle's (MEM) biological mediums were characterized by means of DLS with Photocor-FC spectrometer. A total of 1 ml of 10 mM water colloid solution of Pr^{3+}:LaF_3 (C_{Pr} = 1%) nanoparticles were added to 4 ml of distilled water and Eagle's (MEM) biological medium. After 10 min of sonication (ultrasonic cleaner model UD100SH-2LQ, ultrasonic power 100 W), the suspensions became homogeneous by necked eye, and, then, after 1 h, all the necessary measurements were carried out.

The luminescence spectra were recorded using CCD spectrometer (StellarNet), which detects the emission in 200–1100 nm spectral range with a spectral resolution of 0.5 nm. The optical parametric oscillator laser system (420–1200 nm) from JV LOTIS TII was used for excitation of the luminescence of the samples. The pulse width and the pulse repetition rate were 10 ns and 10 Hz, respectively. The spectral width of laser radiation was less than 0.15 nm. The experiments were carried out at room temperature.

Cell preparation and cytotoxicity assessment of Pr^{3+}:LaF_3 (C_{Pr} = 1%) nanoparticles

The cells were purchased in Russian collection of vertebrate cell cultures, Russian Academy of Sciences, St. Petersburg, Russia. Lung carcinoma (A 549), Madin–Darby canine kidney (MDCK), and lung epithelial of cow (LEC)were cultured in Eagle's (MEM) biological medium with Hank's salts supplemented with 10% fetal calf serum (HyClone, Australia), glutamine (2 mM), and penicillin and streptomycin (100 IU/mL) at 37 °C in 5% CO_2 humidified atmosphere.

The cytotoxicity of the nanoparticles was analyzed via the colorimetric MTT assay. The test protocol for cytotoxicity evaluation was adopted from elsewhere (Kamma et al. 2009). Nanoparticle

suspension in distilled water was added to the cultural medium in a ratio of 1/10 (*v*/*v*) for each concentration. Then, the obtained suspension was sonicated for 10 min until the suspension appeared homogeneous to the necked eye. The cells were treated with the nanoparticles at 0.5, 1, 2.5, and 5 mM. Exposure time was 24 h at 37 °C in humid air (98%) containing 5% CO_2. Three hours prior to the end of the exposure period, MTT (3-(4,5-dimethyl-2-thiazolyl)-2,5-diphenyl-2Htetrazolium bromide, Sigma-Aldrich, #M5655) solution in PBS (5 mg/ml, 20 μl/well) was added to the cells. After the completion of the exposure period, the supernatant was removed, and 100 μl/well solution containing 10% SDS (Sigma-Aldrich, #L3771) in PBS was added. Absorbance at 570 nm of each well was measured using a microplate reader (Biorad, xMark). Each experiment was repeated 2 times, with five replications. The incubation time (120 min) for internalization study was measured between the moment of adding the NPs and the moment of fixing by glutaraldehyde or between the moment of adding the NPs and the moment of performing flow cytometry experiments.

Flow cytometry

In this work, the possibility of internalization of Pr^{3+}:LaF_3 (C_{Pr} = 1%) nanoparticles by the A549, MDCK, and LEC cells was investigated via flow cytometry. The cell monolayer was trypsinized, and the cell suspension was precipitated by centrifugation (1500 rpm, 5 min). The supernatant was removed, the cells were resuspended in a complete Eagle's (MEM) medium at a concentration of 10^6 cells/ml, and a suspension of nanoparticles in distilled water was added. The final concentration of the nanoparticles was 0.1 g/l for all cases. The incubation time of the nanoparticles and cells was 120 min. A cytometric assessment of the internalization of nanoparticles by cells was performed using flow cytometry, analyzing changes in the intensity of side scattering signal (SSC) of the cells. The value of the SSC is proportional to cell granularity. During the experiments, we compared values of SSC of untreated cells and cells treated by the NPs. FACSCanto II cytofluorometer (BD, USA) was used in the work. The initial processing of the results was performed using the FACSDiva Software (BD) program.

Transmission electron microscopy

Sample preparation: 10 μl of the suspension was placed on a formvar/carbon lacey 3 mm copper grid, and drying was performed at room temperature. After drying, the grid was placed in a transmission electron microscope using special holder for microanalysis. Analysis was held at an accelerating voltage of 100 kV in TEM mode, and the elemental analysis was carried out in STEM mode, at the same parameters using Oxford Instruments X-Max™ 80 T detector. Analysis of Pr^{3+}:LaF_3 (C_{Pr} = 1%) nanoparticles was carried out in a transmission electron microscope Hitachi HT7700 Exalens.

The control of amount of nitrates in colloidal solution of the nanoparticles after each stage of centrifugation was performed by identification test using diphenylamine (diphenylamine test).

Preparation of the samples of A549, LEC, and MDCK cells treated by Pr^{3+}:LaF_3 (C_{Pr} = 1%) nanoparticles for TEM was carried out as follows:

1) Separate the cells from the incubation medium by centrifuging for 5 min at 1000 rpm;
2) The supernatant containing non-cell-bound nanoparticles was removed, resuspended in PBS, and then centrifuged again, repeating it three times;
3) After the cells were resuspended in 1 ml of PBS, 1.5 ml was transferred to the Eppendorf;
4) Centrifuged at 4000 rpm in an Eppendorf 5412 microcentrifuge for 5 min;
5) The supernatant was carefully removed, 1.5 ml of glutaraldehyde was added, and it was left at + 4 °C.
6) Samples (system "cells + nanoparticles") were prepared for TEM.

The samples were fixed overnight in 2.5% glutaraldehyde prepared in 0.1 M phosphate buffer (pH 7.2) at 4 °C, washed three times with 0.1 M phosphate buffer, and post-fixed by incubation in 1% (*w*/*v*) osmium tetroxide in the same buffer (25 mg/ml) at 4 °C for 4 h. The samples were dehydrated by passage through a graded ethanol series (30, 40, 50, 60, 70, 80, 90, and then 96% ethanol) before being transferred to 100% acetone and propylene oxide. Then, the samples were immersed in Epon resin (Fluka, Buchs, Switzerland)

that contained propylene oxide added in proportions (*v*/*v*) 1:2, 1:1, and 2:1, with each step involving a 12-h incubation. The samples were then embedded in pure Epon resin. Ultrathin sections (ca. 100 nm) were prepared using a glass knife on a Leica UC7, mounted on 200 mesh copper grids, and stained with 2% aqueous uranyl acetate (*w*/*v*) for 20 min and Reynolds' lead citrate (Reynolds 1963) for 7 min. The sections were examined using a transmission electron microscope (HT 7700 Exalens, Hitachi, Japan) operated at an accelerating voltage of 100 kV.

Results and discussion

Pr^{3+}:LaF_3 ($C_{Pr} = 1\%$) nanoparticle characterization

Transmission electron microscopy (TEM) data indicate that obtained Pr^{3+}:LaF_3 ($C_{Pr} = 1\%$) samples consist of nearly monodisperse well-crystallized nanoparticles. The shape of the nanoparticles is not perfectly spherical. An average nanoparticle diameter is 14 ± 2 nm (Fig. 1). Selected area electron diffraction (SAED) patterns (Fig. 2) correspond to hexagonal crystal structure and do not contain any reflections from impurity phases. The presence of circular rings in the SAED patterns indicates polycrystallinity of Pr^{3+}:LaF_3 samples. No signs of orientation ordering or oriented attachment of the nanoparticles are observed. According to the X-ray diffraction data (Fig. 3a), the Pr^{3+}:LaF_3 ($C_{Pr} = 1\%$) nanoparticles were hexagonal-structured nanocrystals. Sharp peaks of the patterns (full-width at half-maximum (FWHM) of (111) peak is $0.512 \pm 0.003°$) confirm good crystallinity of the nanoparticles. The lattice parameters for Pr^{3+}:LaF_3 ($C_{Pr} = 1\%$) nanoparticles are $a = 7.123(2)$ Å and $c = 7.297(4)$ Å. These values are different from the lattice parameters for LaF_3 (JCPDS-32-0483) $a = 7.7186$ Å and $c = 7.352$ Å because of the crystal lattice distortion. The radius of Pr^{3+} (1.05 Å) is smaller than that of La^{3+} (1.13 Å) due to the lanthanide contraction, so the cell volume of Pr^{3+}:LaF_3 reduces with more Pr^{3+} replacing La^{3+}. The average nanoparticle size was calculated using Debye–Scherrer's formula:

$$D = \frac{K\lambda}{\beta_{hkl}\mathrm{Cos}\theta}$$

where D is a mean size of NP, K is a shape factor (we used $K = 0.9$), λ is the X-ray wavelength (0.15418 nm), β_{hkl} (111) is the line broadening at half the maximum intensity (FWHM) in radians, and θ is the Bragg's angle (in °). The D values of all the nanoparticles are around 12 nm which is in good accordance with HR TEM data. It can be concluded that the peak broadening of the XRD spectra is mainly related to the nanoscale dimensionality of the crystalline particles.

According to DLS data, more than 90% of Pr^{3+}:LaF_3 ($C_{Pr} = 1\%$) nanoparticles have the mean hydrodynamic radius in distilled water around 45 ± 5 nm, and it does not change at least 21 days. The quantity of the agglomeration of the nanoparticles with mean hydrodynamic radius more than 1000 nm is less than 10%. These facts indicate a very low

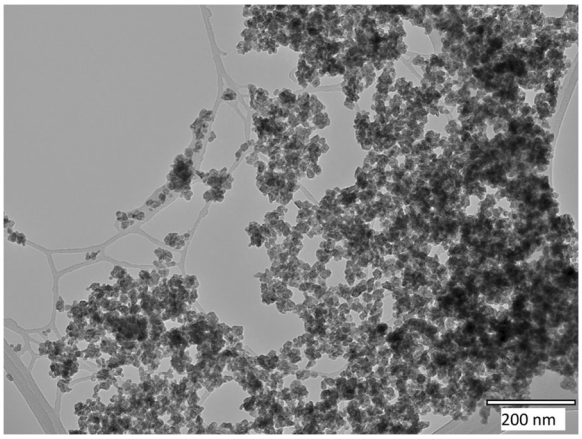

Fig. 1 TEM image of the Pr^{3+}:LaF_3 ($C_{Pr} = 1\%$) nanoparticles

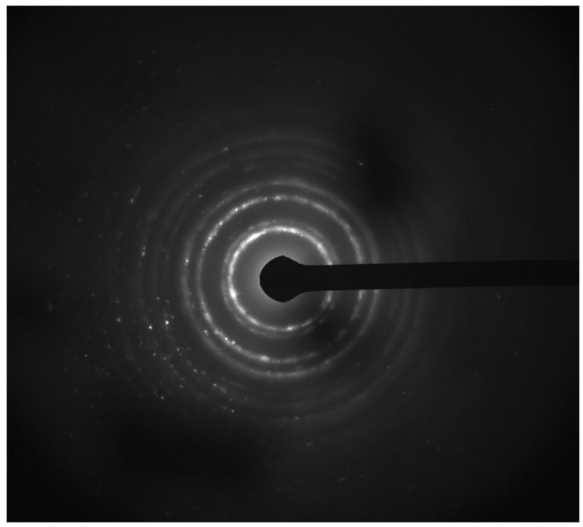

Fig. 2 SAED patterns of the Pr^{3+}:LaF_3 ($C_{Pr} = 1\%$) nanoparticles

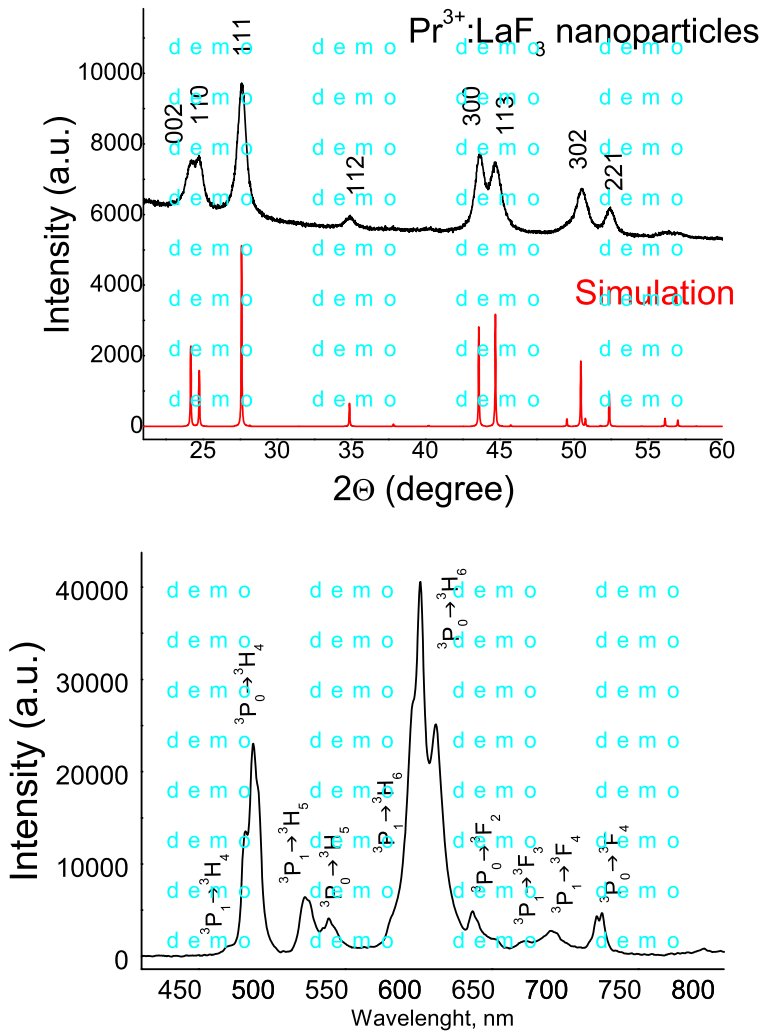

Fig.3 **a** X-ray diffraction patterns of the Pr^{3+}:LaF_3 ($C_{Pr} = 1\%$) nanoparticles. **b** Luminescence spectrum of the Pr^{3+}:LaF_3 ($C_{Pr} = 1\%$) nanoparticles obtained at room temperature (excitation wavelength $\lambda_{ex} = 444$ nm)

degree of huge agglomeration of the nanoparticles in distilled water colloid solution. In Eagle's (MEM) biological medium, more than 90% of Pr^{3+}:LaF_3 ($C_{Pr} = 1\%$) nanoparticles have the hydrodynamic radii about 110 ± 6 nm. Furthermore, only 6% of the particles are huge (> 1000 nm) agglomerates. The value of the mean hydrodynamic radius is notably more than the mean nanoparticles' physical radius, obtained via TEM. It can be suggested that nanoparticles form small agglomerates as was shown in Ma et al. (2007) via TEM. Also, it should be noted that unlike TEM, hydrodynamic radius does not determine the physical size of the nanoparticle. The hydrodynamic radius steams from the Stocks–Einstein equation in DLS method (Lim et al. 2013).

The EDX spectroscopy indicates that the Pr^{3+}:LaF_3 ($C_{Pr} = 1\%$) nanoparticles contain Pr, La, and F. Additionally, the diphenylamine test did not reveal presence of nitrates in the nanoparticles' colloidal solution after the third stage of centrifugation. According to both methods, 5 stages of centrifugation (12,000 revolutions/min for 10 min) in water guarantee thorough absence of nitrates and other substances.

Room temperature luminescence spectrum of Pr^{3+}:LaF_3 ($C_{Pr} = 1\%$) nanoparticles excited by pulse laser beam at 444 nm is presented in Fig. 3b. The luminescent spectra have the emission bands at about 487, 523, 537, 580, 601, and 672 nm which are interpreted as the result of the transition from ^3P_j (j = 0, 1, 2) excited states to $^3H_4$, $^3H_5$, $^3H_5$, $^3H_6$, and $^3F_4$ states

of Pr^{3+}ions, respectively. The emission bands corresponding to impurities or any unidentified bands are not found.

The TEM images of the A 549, MDCK, and LEC cells (control)

TEM images of A 549, MDCK, and LEC cells not exposed by the nanoparticles are shown in Fig. 4a, b, and c, respectively. These TEM images serve as control.

The A 549, MDCK, and LEC cells have a polygonal shape and sheet-like pattern in normal monolayer culture, which is compatible with its epithelial origin (Stearns et al. 2001). It is clearly seen that the cell membrane has distinguishing structural features, including different shapes of membrane protrusions for all the above-mentioned cell lines. Most of these protrusions are planar folds (lamellipodia-like) with length from 100 to 500 nm, and the rest of them are plasma membrane extrusions (blebs) having diameter of 30–60 nm. Almost the same cell membrane structural features of A 549 cell line were observed in Stearns et al. (2001). The cytoplasm contains vesicles having diameter from 200 to 500 nm. Apparently, these vesicles are formed by the above-mentioned membrane protrusions which fused back into the membrane and trapped extracellular fluid.

The A 549, MDCK, and LEC uptake and cytotoxicity of the Pr^{3+}:LaF_3 ($C_{Pr} = 1\%$) nanoparticles

Although the chosen cell lines are epithelial, they demonstrate notably different uptake efficiency. It seems that the A 549 cells internalize the nanoparticles more effectively. Nevertheless, after 2 h of nanoparticle exposure A 549, MDCK, and LEC cells (Figs. 5, 6, and 7, respectively) internalized the nanoparticles and 20–300 nm agglomerates of the nanoparticles packed into 200–500 nm vesicles were found into the cytoplasm. It seems that the internalization occurs via macropinocytosis classified as the endocytic process by which cells internalize fluids and particles together. During macropinocytosis, relatively large vesicles (0.2–5 μm) are formed (Kuhn et al. 2014 Froehlich & Roblegg 2014, Irvine et al. 1999). The internalization occurs via macropinosomes which are 100–300 nm in length (for example, Fig. 5a). Other types of endocytosis were not observed via TEM under the experimental conditions. However, in the case of A 549 cells, the

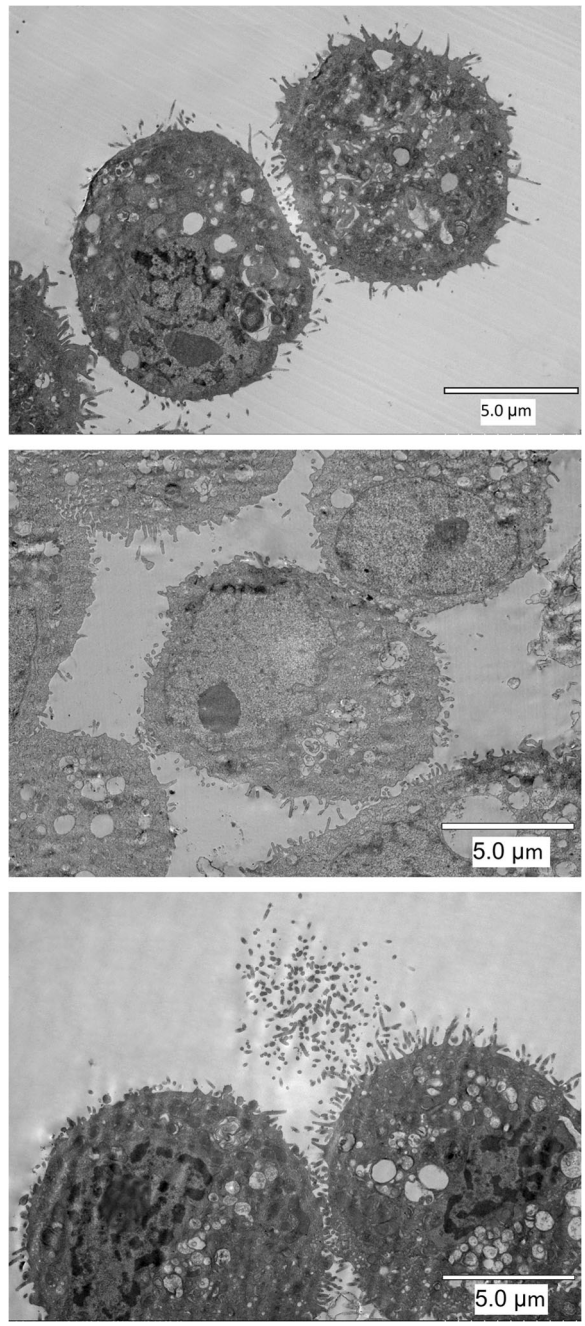

Fig.4 **a** TEM images of A 549 cells. **b** TEM images of MDCK cells. **c** TEM images of LEC cells

nanoparticles not packed into the vesicles were also found (Fig. 5c). Moreover, it is clearly seen in Fig. 5c that one part of the membrane of the vesicle is destroyed and the nanoparticles are escaping the vesicle. Apparently, these freely floating nanoparticles stem from such destroyed vesicles rather than from

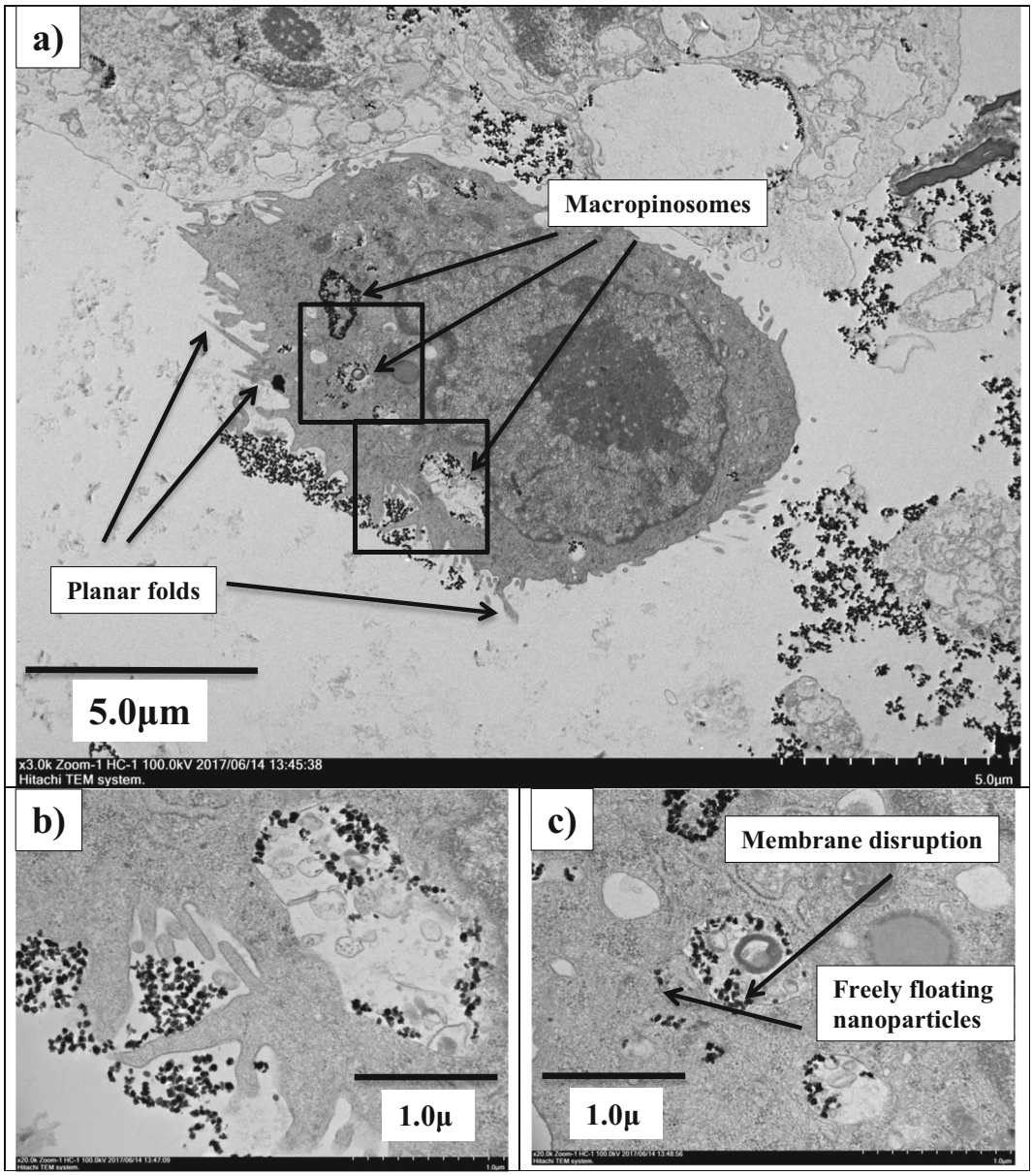

Fig. 5 **a,b,c** TEM images of A 549 cells under nanoparticle exposure

passive cellular membrane penetration. However, such a phenomenon was not observed for MDCK and LEC cells. The process of macropinocytosis of A 549 cells is the most illustrative (Fig. 5b). The two ~220 nm vesicles are seen. One vesicle contains a 180 nm agglomerate of the nanoparticles. The process of capture of the nanoparticles via macropinosome is also clearly observed. The vesicles of LEC cells differ between each other in size more significantly comparing with A 549 cells. These vesicles contain the mean ~50 nm agglomerates of the nanoparticles as well as small agglomerates consisting of a few nanoparticles.

It is noteworthy that the nanoparticles were not found in the cellular organelles under the existing incubation conditions for all the cells. However, the fate of the nanoparticles into the cells requires more precise investigations.

As shown in Fig. 8, in general, the cytotoxicity of the Pr^{3+}:LaF_3 nanoparticles is not significant at

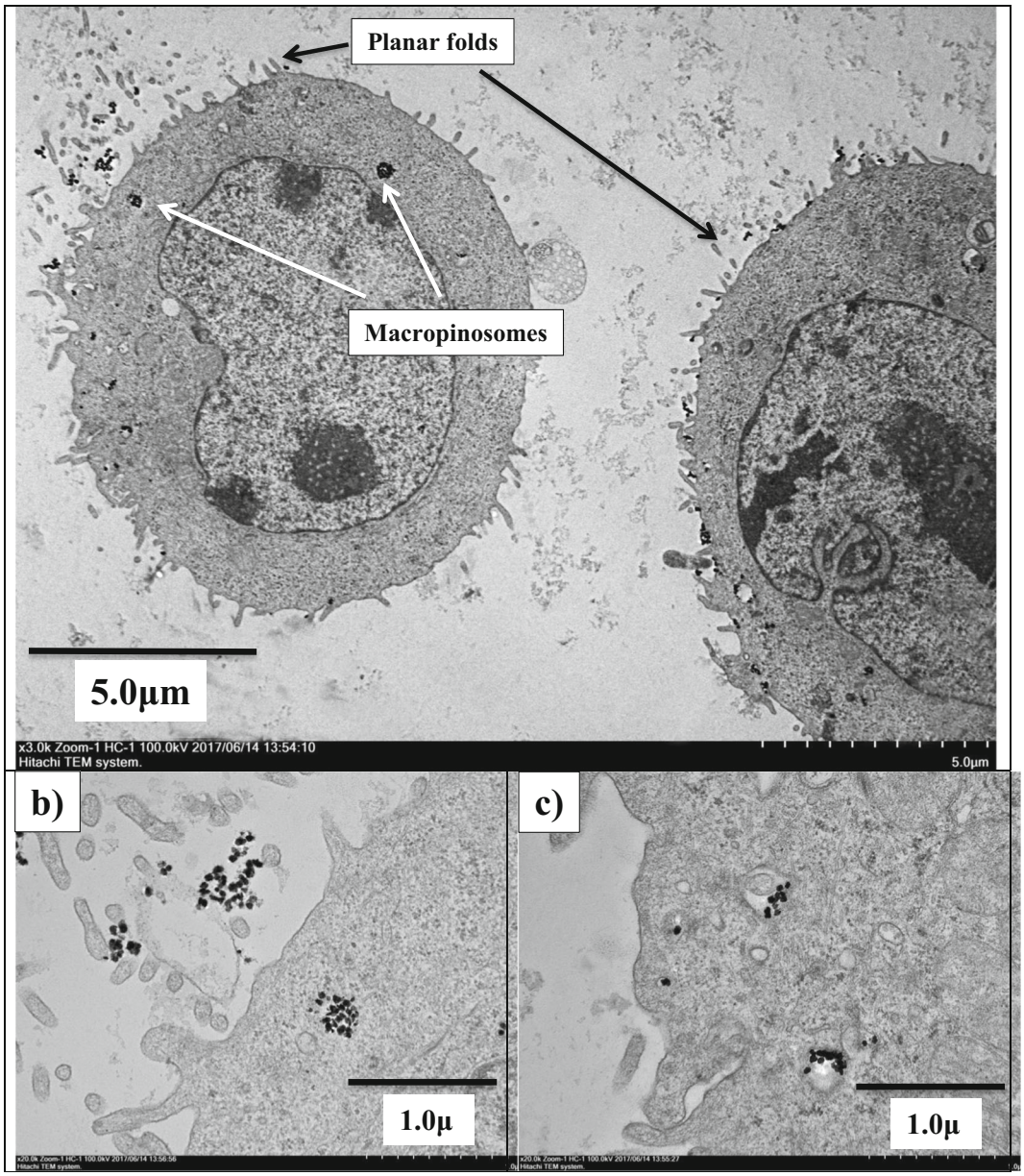

Fig. 6 **a,b,c** TEM images of MDCK cells under nanoparticle exposure

concentrations of 0.05, 0.1, 0.25, and 0.5 g/L. The cytotoxic effect starts from relatively high concentration of 1.0 g/L. In particular, for A 549, LEC, and MDCK cells, the values of survival are around 80% at 1.0 g/L.

Flow cytometry

Additionally, the interaction of the cells and the nanoparticles was studied via flow cytometry. It is well-known that presence of nanoparticles into a cell or their sorption on its membrane increases the SSC intensity (Wysokińska et al. 2016). For A 549, LEC, and MDCK cells treated by nanoparticles, the values of SSC are increased by 16, 39, and 20%, respectively, comparing with the untreated cells. The flow cytometry data are represented in the Supplementary information file. This fact indicates that nanoparticles effectively interact with the cells. However, the distinguishing contributions of internalized or adsorbed nanoparticles require further investigation.

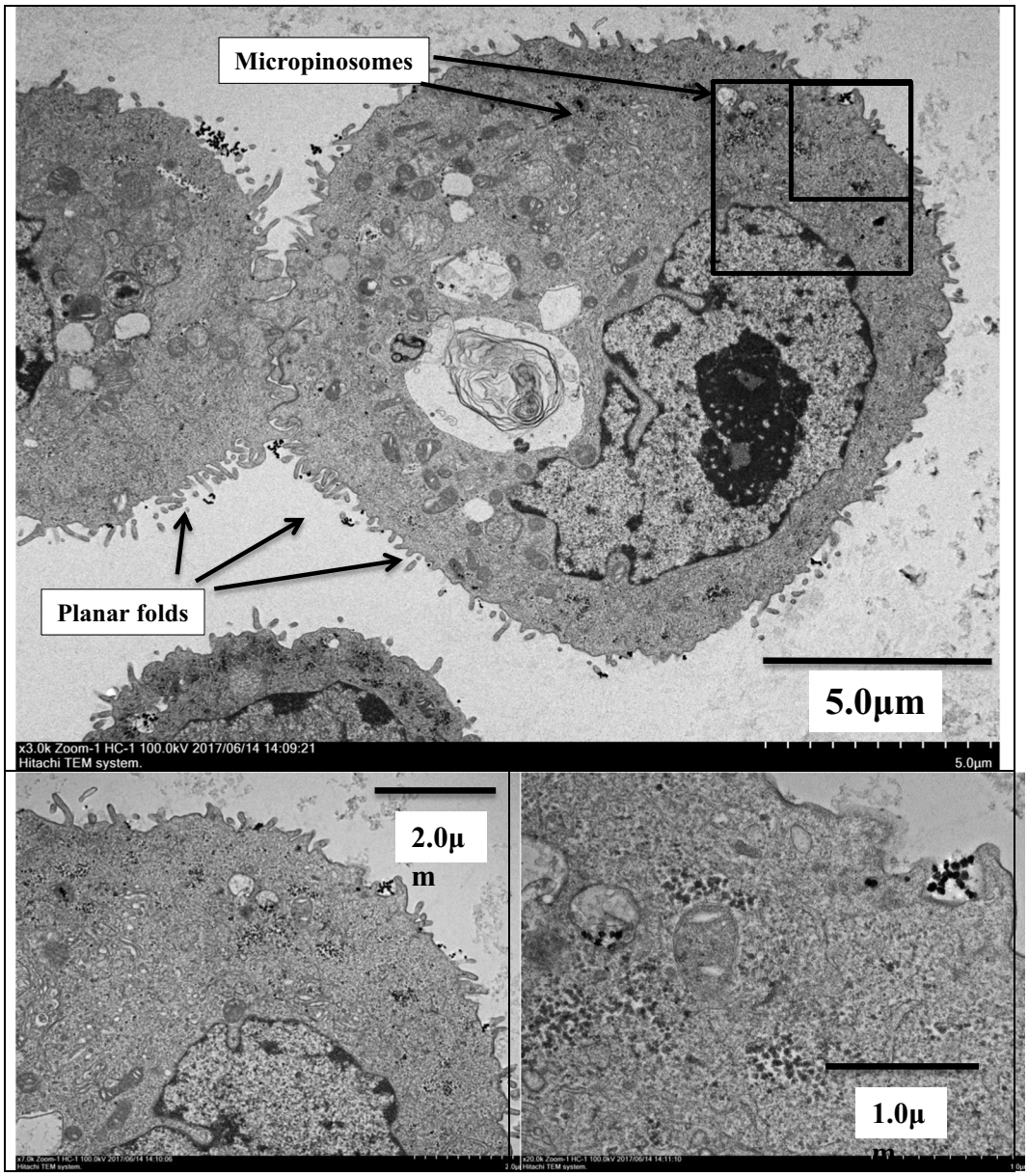

Fig. 7 **a,b,c** TEM images of LEC cells under nanoparticle exposure

Conclusions

The obtained unmodified Pr^{3+}:LaF_3 ($C_{Pr} = 1\%$) nanoparticles were characterized by means of TEM, XRD, DLS, energy-dispersive spectroscopy, and optical spectroscopy. The average diameter of the nanoparticles is 14 nm. The nanoparticles form agglomerates in Eagle's (MEM) biological medium + FBS. The hydrodynamic radius of such agglomerates is around 110 nm. The nanoparticles are hexagonal-structured nanocrystals without any impurities. The luminescent spectra have emission bands at about 487, 523, 537, 580, 601, and 672 nm, which are interpreted as the result of the transition from ^3P_j ($j = 0, 1, 2$) excited states to $^3H_4$, $^3H_5$, $^3H_5$, $^3H_6$, and $^3F_4$ states of Pr^{3+}ions, respectively. According to the energy-dispersive spectroscopy, nanoparticles contain Pr, La, and F only. The nanoparticles form agglomerates in Eagle's (MEM) biological medium + FBS. The hydrodynamic radius of such agglomerates is around 110 nm.

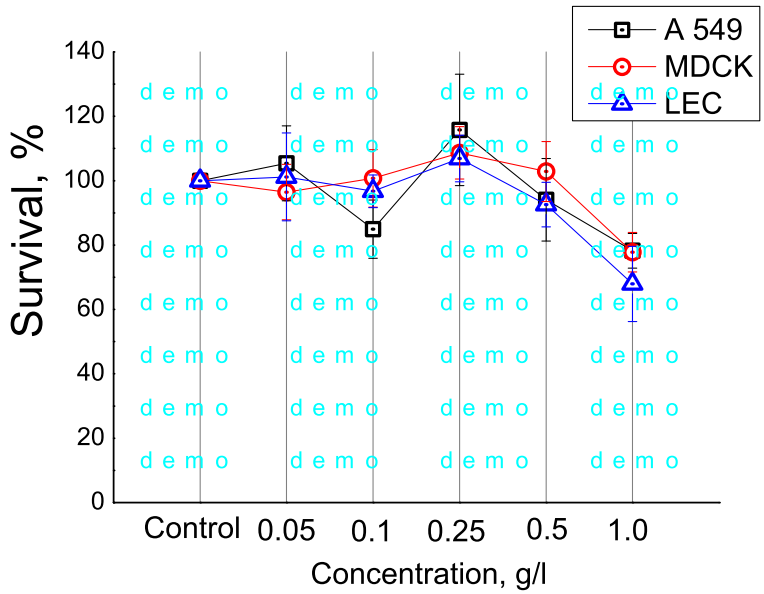

Fig. 8 Relative viability of A 549, LEK, and MDCK cells treated with the Pr^{3+}:LaF_3 nanoparticles at 0.05, 0.1, 0.25, and 0.5 g/L concentrations in comparison to control cells

The nanoparticles are internalized and adsorbed by the A549, MDCK, and LEC cells. However, the features of interaction between the nanoparticles and the A549, MDCK, and LEC cells are different between each other. Specifically, by means of TEM, it was revealed that after 2 h of the nanoparticle exposure, the A 549, MDCK, and LEC cells internalized the nanoparticles and 20–300 nm agglomerates of the nanoparticles packed into 200–500 nm vesicles were found in the cytoplasm. However, it seems that A 549 cells internalize the nanoparticles more effectively. In the case of MDCK and LEC cells, the number of vesicles filled with nanoparticles is noticeably less in comparison to A 549 cells. It seems that the internalization occurs via macropinocytosis.

For the first time, for LaF_3-doped nanoparticles, it was revealed that in the A 549 cells, disruption of some vesicles takes place. This disruption leads to escaping the nanoparticles from the vesicle to the cytoplasm. Hence, freely floating nanoparticles in the cytoplasm are also found. The reactivity of such freely floating nanoparticles can be higher in comparison to nanoparticles packed to vesicles. Hence, these freely floating nanoparticles can have the biggest contribution to the nature of cytotoxicity among other processes. However, it is still a matter of further investigations. Nevertheless, the disruption of some vesicles is not observed for RE-doped $NaLnF_4$ (Ln = Y, Gd). It can be suggested that the surface charge density or another properties and as consequence features of interaction between the studied cells and LaF_3-based NPs are unique and require additional study.

Additionally, the flow cytometry showed that all the cells effectively interact with the nanoparticles. This interaction leads to cell granularity change. Particularly, the A 549, MDCK, and LEC cells treated by nanoparticles have the values of SSC 16 ± 2, 20 ± 3, and 39 ± 3%, respectively, comparing with the untreated cells. The increasing of SSC qualitatively confirms cellular uptake as well as adhesion. Finally, the Pr^{3+}:LaF_3 (C_{Pr} = 1%) nanoparticles were not found into the cellular organelles under the existing incubation conditions for all the cells. However, the fate of nanoparticles into the cell requires more precise investigations.

For the first time, it was revealed that the investigated nanoparticles are relatively low toxic for the chosen cell cultures. The cytotoxic effect starts from a relatively high concentration of 1.0 g/L. In particular, for A 549, LEC, and MDCK cells, the values of survival are around 80% at 1.0 g/L.

Finally, it can be concluded that unmodified Pr^{3+}:LaF_3 (C_{Pr} = 1%) nanoparticles are low toxic. They can be easily uptaken by the A 549, LEC, and MDCK cells and can, as consequence, serve as different probes in different biological applications.

Acknowledgments The biological experiments and TEM microscopy studies were funded by the subsidy allocated to the Kazan Federal University for the state assignment in the sphere

of scientific activities [3.1156.2017/4.6] and [3.5835.2017/6.7]. Microscopy studies were carried out at the Interdisciplinary Center of Analytical Microscopy of the Kazan Federal University. The optical spectroscopy and XRD experiments were funded by the research grant of the Kazan Federal University.

Compliance with ethical standards

Conflict of interest The authors declare that they have no conflict of interest.

References

Alakshin EM, Gazizulin RR, Klochkov AV, Korableva SL, Safin TR, Safiullin KR, Tagirov MS (2014) Annealing of PrF3 nanoparticles by microwave irradiation. Opt Spectrosc 116(5):721–723. https://doi.org/10.1134/S0030400X14050026

Alakshin EM, Klochkov AV, Kondratyeva EI, Korableva SL, Kiiamov AG, Nuzhina DS, Kodjikian S (2016) Microwave-assisted hydrothermal synthesis and annealing of DyF3 nanoparticles. J Nanomater 2016:7148307. https://doi.org/10.1155/2016/7148307

Bekah D, Cooper D, Kudinov K, Hill C, Seuntjens J, Bradforth S, Nadeau J (2016) Synthesis and characterization of biologically stable, doped LaF3 nanoparticles co-conjugated to PEG and photosensitizers. J Photochem Photobiol A Chem 329:26–34. https://doi.org/10.1016/j.jphotochem.2016.06.008

Dong H, Du S, Zheng X, Lyu G, Sun L, Li L, Zhang P, Zhang C, Yan C (2015) Lanthanide nanoparticles: from design toward bioimaging and therapy. Chem Rev 115:10725–10815. https://doi.org/10.1021/acs.chemrev.5b00091

Froehlich E, Roblegg E (2014) Mucus as barrier for drug delivery by nanoparticles. J Nanosci Nanotechnol 14(1):126–136. https://doi.org/10.1166/jnn.2014.9015

Gnach A, Lipinski T, Bednarkiewicz A, Rybka J, Capobianco JA (2015) Upconverting nanoparticles: assessing the toxicity. Chem Soc Rev 44(6):1561–1584. https://doi.org/10.1039/c4cs00177j

Irvine JD, Takahashi L, Lockhart K, Cheong J, Tolan JW, Selick HE, Grove JR (1999) MDCK (Madin–Darby canine kidney) cells: a tool for membrane permeability screening. J Pharm Sci 88(1):28–33. https://doi.org/10.1021/js9803205

Jalil RA, Zhang Y (2008) Biocompatibility of silica coated NaYF4 upconversion fluorescent nanocrystals. Biomaterials 29:4122–4128. https://doi.org/10.1016/j.biomaterials.2008.07.012

Jaque D, Vetrone F (2012) Luminescence nanothermometry. Nanoscale 4(15):4301–4326. https://doi.org/10.1039/c2nr30764b

Kaczkan M, Boruc Z, Fetlinski B, Turczynski S, Malinowski M (2013) Temperature dependence of 3P0 Pr3+ fluorescence dynamics in Y4Al2O9 crystals. Appl Phys B Lasers Opt 113(2):277–283. https://doi.org/10.1007/s00340-013-5469-3

Kamma I, Kommidi P, Reddy BR (2009) High temperature measurement using luminescence of Pr3+ doped YAG and Ho3+ doped CaF2. Phys Status Solidi C 6(S11):S187–S190. https://doi.org/10.1002/pssc.200881334

Kuhn DA, Vanhecke D, Michen B, Blank F, Gehr P, Petri-Fink A, Rothen-Rutishauser B (2014) Different endocytotic uptake mechanisms for nanoparticles in epithelial cells and macrophages. Beilstein J Nanotechnol 5(1):1625–1636. https://doi.org/10.3762/bjnano.5.174

Ladol J., Khajuria H, Khajuria S, Sheikh HN (2016). Hydrothermal synthesis, characterization and luminescent properties of lanthanide-doped NaLaF4 nanoparticles. Bulletin of Materials Science. 39(4): 943-952

Lellouche J, Friedman A, Gedanken A, Banin E (2012) Antibacterial and antibiofilm properties of yttrium fluoride nanoparticles. Int J Nanomedicine 7:5611. https://doi.org/10.2147/IJN.S37075

Lim J, Yeap SP, Che HX, Low SC (2013) Characterization of magnetic nanoparticle by dynamic light scattering. Nanoscale Res Lett 8(1):381. https://doi.org/10.1186/1556-276X-8-381

Ma L, Chen WX, Zheng YF, Zhao J, Xu Z (2007) Microwave-assisted hydrothermal synthesis and characterizations of PrF3 hollow nanoparticles. Mater Lett 61(13):2765–2768. https://doi.org/10.1016/j.matlet.2006.04.124

Misfeldt DS, Hamamoto ST, Pitelka DR (1976) Transepithelial transport in cell culture. Proc Natl Acad Sci 73(4):1212–1216. https://doi.org/10.1073/pnas.73.4.1212

Nel AE, Mädler L, Velegol D, Xia T, Hoek EM, Somasundaran P, Thompson M (2009) Understanding biophysicochemical interactions at the nano–bio interface. Nat Mater 8(7):543. https://doi.org/10.1038/nmat2442,557

Oh N, Park JH (2014) Endocytosis and exocytosis of nanoparticles in mammalian cells. Int J Nanomedicine 9(Suppl 1):51

Pudovkin MS, Koryakovtseva DA, Lukinova EV, Korableva SL, Khusnutdinova RS, Kiiamov AG, Nizamutdinov AS, Semashko VV (2019) Characterization of Pr-doped LaF3 nanoparticles synthesized by different variations of coprecipitation method. J Nanomater 2019:7549325. https://doi.org/10.1155/2019/7549325

Pudovkin MS, Morozov OA, Pavlov VV, Korableva SL, Lukinova EV, Osin YN, Evtugyn VG, Safiullin RA, Semashko VV (2017) Physical background for luminescence thermometry sensors based on Pr3+:LaF3 crystalline particles. J Nanomater 2017:3108586. https://doi.org/10.1155/2017/3108586

Pudovkin MS, Zelenikhin PV, Krasheninnikova AO, Korableva SL, Nizamutdinov AS, Alakshin EM, Semashko VV, Safiullin RA, Kadirov MK (2016) Photoinduced toxicity of PrF3 and LaF3 nanoparticles. Opt Spectrosc 121(4):538–543. https://doi.org/10.1134/S0030400X16100209

Pudovkin MS, Zelenikhin PV, Shtyreva V, Morozov OA, Koryakovtseva DA, Pavlov VV et al (2018) Coprecipitation method of synthesis, characterization, and cytotoxicity of Pr3+: LaF3 (CPr = 3, 7, 12, 20, 30%) nanoparticles. J Nanotechnol 2018:8516498. https://doi.org/10.1155/2018/8516498

Rai VK, Rai DK, Rai SB (2006) Pr3+ doped lithium tellurite glass as a temperature sensor. Sensors Actuators A Phys 128(1):14–17. https://doi.org/10.1016/j.sna.2005.12.030

Rakhmatullin RM, Pudovkin MS, Semashko VV (2019) EPR evidence of surface paramagnetic defects formation due to

annealing of LaF3 nanoparticles. Magnetic resonance in solids. Electron J 21:4. https://doi.org/10.26907/mrsej-19411

Reynolds ES (1963) The use of lead citrate at high pH as an electron-opaque stain in electron microscopy. The Journal of cell biology. 17(1): 208.

Ribeiro AR, Gemini-Piperni S, Travassos R, Lemgruber L, Silva RC, Rossi AL et al (2016) Trojan-like internalization of anatase titanium dioxide nanoparticles by human osteoblast cells. Sci Rep 6:23615. https://doi.org/10.1038/srep23615

Sahu D, Kannan GM, Tailang M, Vijayaraghavan R (2016) In vitro cytotoxicity of nanoparticles: a comparison between particle size and cell type. J Nanosci 2016:9. https://doi.org/10.1155/2016/4023852

Semashko VV, Pudovkin MS, Cefalas AC, Zelenikhin PV, Gavriil VE, Nizamutdinov AS, Kollia Z, Ferraro A, Sarantopoulou E (2018) Tiny rare-earth fluoride nanoparticles activate tumour cell growth via electrical polar interactions. Nanoscale Res Lett 13(1):370. https://doi.org/10.1186/s11671-018-2775-z

Shcherbakov AB, Zholobak NM, Baranchikov AE, Ryabova AV, Ivanov VK (2015) Cerium fluoride nanoparticles protect cells against oxidative stress. Mater Sci Eng C 50:151–159. https://doi.org/10.1016/j.msec.2015.01.094

Stearns RC, Paulauskis JD, Godleski JJ (2001) Endocytosis of ultrafine particles by A549 cells. Am J Respir Cell Mol Biol. 24(2):108–115. https://doi.org/10.1165/ajrcmb.24.2.4081

Verma A, Stellacci F (2010) Effect of surface properties on nanoparticle–cell interactions. Small 6(1):12–21. https://doi.org/10.1002/smll.200901158

Wang K, Ma J, He M, Gao G, Xu H, Sang J, Cui D (2013) Toxicity assessments of near-infrared upconversion luminescent LaF3:Yb,Er in early development of zebrafish embryos. Theranostics 3(4):258. https://doi.org/10.7150/thno.5701

Wysokińska E, Cichos J, Zioło E, Bednarkiewicz A, Strządała L, Karbowiak M, Hreniak D, Kałas W (2016) Cytotoxic interactions of bare and coated NaGdF4: Yb3+: Er3+ nanoparticles with macrophage and fibroblast cells. Toxicol in Vitro 32:16–25. https://doi.org/10.1016/j.tiv.2015.11.021

Ximendes EC, Rocha U, Kumar KU, Jacinto C, Jaque D (2016) LaF3 core/shell nanoparticles for subcutaneous heating and thermal sensing in the second biological-window. Appl Phys Lett 108(25):253103. https://doi.org/10.1063/1.4954170

Xing H, Bu W, Ren Q, Zheng X, Li M, Zhang S, Zhou L (2012) A NaYbF4: Tm3+ nanoprobe for CT and NIR-to-NIR fluorescent bimodal imaging. Biomaterials 33(21):5384–5393. https://doi.org/10.1016/j.biomaterials.2012.04.002

Yang JM, Yang H, Lin L (2011) Quantum dot nano thermometers reveal heterogeneous local thermogenesis in living cells. ACS Nano 5(6):5067–5071. https://doi.org/10.1021/nn201142f

Zhou J, Yu M, Sun Y, Zhang X, Zhu X, Wu Z, Li F (2011) Fluorine-18-labeled Gd3+/Yb3+/Er3+ co-doped NaYF4 nanophosphors for multimodality PET/MR/UCL imaging. Biomaterials 32(4):1148–1156. https://doi.org/10.1016/j.biomaterials.2010.09.071